A Spatiotemporal Model of Polarity and Spatial Gradient Establishment in *Caulobacter crescentus*

Chunrui Xu
Genetics, Bioinformatics, and Computational Biology
Virginia Tech
Blacksburg, VA, USA
rachelxu@vt.edu

Yang Cao†
Department of Computer Science
Virginia Tech
Blacksburg, VA, USA
ycao@cs.vt.edu

ABSTRACT

Bacterial cells have sophisticated intracellular organization of proteins in space and time, which allow for stress response, signal transduction, cell differentiation and morphogenesis. The mechanisms of spatial localization and their contributions to cell development and adaptability are not fully understood. In this work, we use the bacterial model organism, *Caulobacter cescentus*, to investigate the establishment of polarity and asymmetry. We apply a reaction-diffusion model to simulating spatiotemporal dynamics of scaffolding proteins PodJ and PopZ, which account for the formation of distinct poles in *C. crescentus*. Additionally, we use this mathematical model to investigate the nonuniform distribution of key kinase DivJ and phosphatase PleC and figure out their contributions to the spatial gradient of response regulators DivK and CtrA.

CCS CONCEPTS

• Insert CCS text here • Insert CCS text here • Insert CCS text here

KEYWORDS

Scaffolding proteins, Spatial gradient, asymmetric cell cycle, Reaction-diffusion model

ACM Reference format:

Chunrui Xu, Yang Cao. 2021. A Spatiotemporal Model of Polarity and Asymmetry Establishment of *Caulobacter crescentus*. In *Proceedings of ACM conference on Bioinformatics, Computational Biology, and Health Informatics. ACM-BCB 2021, Virtual*

1 Introduction

Caulobacter crescentus is an oligotrophic Gram-negative bacterium which inhabits aquatic environments. *C. crescentus* becomes a model organism for the study of cell development and differentiation in prokaryotes because it has trackable cell cycle progression, and it can be easily cultivated and synchronized [1]. *C. crescentus* undergoes a dimorphic cell cycle process, resulting in two distinct progenies: a sessile stalked cell that is replicable, and a motile non-replicable swarmer cell that moves away and differentiates into the stalked morphology given suitable environments (Fig. 1). The causes of asymmetric cell cycle of *C. crescentus* are the asymmetric localization and timed interactions of many regulatory proteins [14]. The spatiotemporal regulatory system allows complex processes of *C. crescentus*, such as morphogenesis, cytokinesis, and asymmetrical cell division [14].

Advanced microbial techniques have revealed temporal changes of several landmark proteins during cell cycles of *C. crescentus*, which motivate system biologists to quantitatively investigate the underlying control mechanisms of the *Caulobacter* cell cycle. Li *et al.* [18,19] have constructed mathematical models of master regulators in *C. crescentus*, including CtrA, DnaA, GcrA, and CcrM. Their models capture the main characteristics of DNA replication and methylation in wild type and mutant strains. Murray *et al*. [21] proposed a concise model with CtrA and GcrA and involved phosphorylation of CtrA by CckA. On the other hand, although the temporal cell cycle regulation has been well investigated, the study of cell asymmetry established by spatial distributions of regulators is quite limited.

The spatial orchestration is often accomplished by scaffolding proteins, which control the localization, interaction, and even activities of client proteins [12]. A recent research indicates that PodJ and PopZ function as scaffolding proteins and recruit client proteins at opposite poles, resulting in the asymmetry of *C. crescentus* [12]. One open question here is how PodJ and PopZ themselves localize at specific areas. Several hypotheses have been proposed to explain this initial polar localization. For example, one suggest that as *C. crescentus* is crowded by chromosome, nucleoid occlusion may cause polar accumulation because only poles can provide sufficient space for the protein assembly [12]; others suggest the specific recognition of polar curvature [7] and/or unique elements such as lipid [25] or peptidoglycan [17] composition can cause polar localization. However, these mechanisms cannot explain all scenarios, such as the specific monopolar accumulation and ectopic non-polar accumulation.

†Correspondence.

ACM-BCB'21, August 1-4, 2021, Virtual

Additionally, the master regulator CtrA shows spatial gradient throughout cells. Phosphorylated CtrA controls the transcription of more than 100 genes in *C. crescentus*, many of which regulate the polar morphogenesis and cell division. CtrA~P also binds to *Cori* to inhibit DNA replication [16]. Therefore, a high level of CtrA~P in swarmer cell and a low level in stalked cell determine different fates of distinct progenies [30]. The CtrA~P gradient is likely caused by activity and abundance regulations [4,9]; however specific mechanisms are yet well elucidated.

Subramanian *et al* [27] proposed a modified Turing model to investigate the mechanism of spatial dynamics of PopZ. An unknown nucleating factor, likely PodJ with support of new evidence, is required for the second focus of PopZ formation in the Turing model. In this paper, we applied a similar Turing model to investigating the mechanism of the first polar localization of PodJ. We propose a novel reaction-diffusion model to capture the spatiotemporal dynamics of scaffolding proteins PodJ and PopZ as well as key client proteins including SpmX, PleC, and DivJ. Our *in silico* model of two signaling hub at opposite poles are based on the two scaffolding proteins PodJ and PopZ. Kinase DivJ and phosphatase PleC are directly or indirectly recruited by PopZ and PodJ, localizing at opposite poles. Polarly distributed PleC and DivJ then contribute to the spatial gradient of CtrA through its mediator DivK. Our model explains the non-uniformly distribution of landmark proteins and provides insights into morphogenesis, cell differentiation, and asymmetry establishment in bacteria.

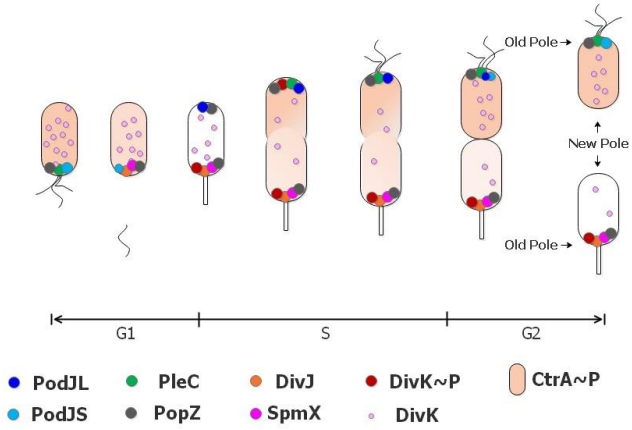

Figure 1. Cell cycle of *C. crescentus* and localization of regulators. Two distinct progenies are produced after cell division. The flagellated swarmer cell differentiates into the stalked morphology (G1-S transition), while the stalked cell can replicate DNA immediately. Scaffolding proteins PodJ and PopZ localize at indicated pole(s) and specifically recruit client proteins such as PleC and SpmX. Most DivK~P localize at the stalked pole whereas CtrA~P is mostly distributed in the swarmer cell/compartment.

2 Method

2.1 General Equation of Reaction-Diffusion Model and Four-compartment Discretization

We use reaction-diffusion equations to capture the spatial and temporal dynamics of proteins [11]

$$\frac{\partial C}{\partial t} = Reaction\ terms + D\frac{\partial^2 C}{\partial x^2},$$

where C indicates the concentration of species S. D represents the diffusion rate of species S.

We apply a compartment-based scheme to convert continuous equations into discrete compartments to achieve quick solution of the corresponding PDEs, the compartment-based scheme also allows us to extend this model to its stochastic version in our future work. Here the number of compartments directly influence the solution accuracy and time complexity. At the initial stage of the investigation, in order to effectively test feasibility and rationality of our model, we choose a 1-D four-compartment model, which can capture major features of *Caulobacter* cell including poles and midcell (Fig. 2). In this four-compartment model, polar compartment accounts for 20% of total cell length (L), while the length of central compartment is 30%L. At the boundary between two adjacent compartments with different sizes, the diffusion flux is proportional to the inverse of distance between centers of two compartments. For example, the jumping rate of a molecule from the 2nd to the 1st compartment is $\frac{D}{h^2}$, where $h=(l_1+l_2)/2$. Take the 2nd compartment as an example, we include molecules jumping into and out the 2nd compartment from/to adjacent 1st/3rd compartments (Fig. 2, arrows). Therefore, the diffusion term can be written as follows:

$$\frac{D}{(\frac{l_2+l_1}{2})^2}(C_1 - C_2) + \frac{D}{(\frac{l_2+l_3}{2})^2}(C_3 - C_2)$$

As we do not consider molecules across cell membrane, there is no molecule jumping between extra cellular area and cytoplasm in our model. Diffusion term of 4-compartment is summarized as follows:

$$\begin{cases} D\cdot\frac{\partial^2 C_1}{\partial x^2} = \frac{D(C_2 - C_1)}{(\frac{l_2+l_1}{2})^2} \\ D\cdot\frac{\partial^2 C_i}{\partial x^2} = \frac{D(C_{i+1} - C_i)}{(\frac{l_{i+1}+l_i}{2})^2} + \frac{D(C_{i-1} - C_i)}{(\frac{l_{i-1}+l_i}{2})^2}, \quad i = 2,3 \\ D\cdot\frac{\partial^2 C_4}{\partial x^2} = \frac{D(C_3 - C_4)}{(\frac{l_3+l_4}{2})^2} \end{cases}$$

where C_i indicates the concentration of species S in the ith compartment and l_i indicates the length of compartment i. We assume each compartment grows exponentially with time. The growth rate (μ) is estimated based on measured cell size over cell cycle [28].

$$\frac{dl}{dt} = \mu l$$

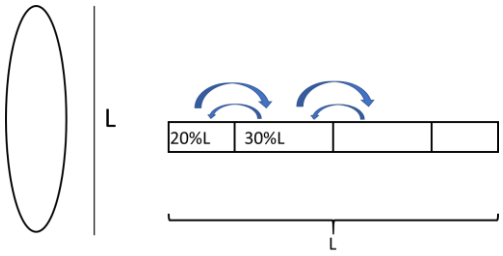

Figure 2. 1-D 4-compartment method divides the entire cell (size=L) into 4 compartments with 20% for poles and 30% for central fields. Blue arrows indicate molecules jumping between 2nd compartment and its adjacent compartments.

2.2 Turing Model of PodJ and PopZ

The Turing model is a well-known mechanism to explain self-regulated pattern formation in biological issues [11]. A stable Turing pattern can be generated by a production-substrate deletion system if the following criteria are satisfied [11]:

a). One species is the product with autocatalytic reaction and has a slow diffusion rate.

b). One species is the substrate which has a sufficiently high diffusion rate.

Subramanian *et al* [27] has applied a Turing model to simulate the bipolar pattern of PopZ in *C. crescentus* (Fig. 1, gray) using polymer as the product and monomer as the substrate. While the old pole accumulation of PopZ is inheritance from mother cell, the reason of stable new focus of PopZ at the opposite pole was discussed but not ensured in their model. Here, we applied a similar Turing model to PodJ and SpmX, with improvement to Subramanian *et al*'s PopZ model to build the foundation of opposite polar signaling hubs in *C. crescentus*.

Experimental observations suggest that PodJ and SpmX also have characteristics satisfying criteria of Turing pattern formation. Both PodJ and SpmX are verified to oligomerize and self-assemble in cells, where the polymer form should diffuse substantially slower than monomer because of higher mass [13,22,27,32]. Additionally, the interactions among PopZ, PodJ, and SpmX may contribute to the polarized distribution for these three proteins. It has been reported that PodJ is required for the second accumulation of PopZ at the new pole [32], which is likely the unknown nucleating factor mentioned in Subramanian *et al*'s model. PopZ localizes SpmX at the old pole, while SpmX shows inhibitory function on the localization of PodJ [32] (Fig. 3).

Unlike PopZ, which has bipolar accumulation, PodJ localizes at one specific pole. Long form PodJ ($PodJ_L$) only accumulates at the new pole (Fig. 1, dark blue) and is truncated by the protease PerP to become short form PodJ ($PodJ_S$) in the late predivisional cell (Fig. 1, light blue). $PodJ_S$ is then proteolyzed during the swarmer to stalk (sw-to-st) transition in the next cycle, before new $PodJ_L$ being synthesized and accumulated at the opposite pole. PodJ is the only known scaffolding protein at the new pole, recruiting a series of client proteins such as PopZ and PleC [12]. The recruitment by PodJ at the new pole contributes to the second polar focus of PopZ. Therefore, we added PodJ recruitment into Subramanian *et al*'s PopZ model as follows:

$$\frac{d[\mathrm{PopZ_m}]}{dt} = k_{\mathrm{s,PopZ}} - \left(k_{\mathrm{d,PopZ}} + \mu\right)\cdot[\mathrm{PopZ_m}] - k_{\mathrm{dnv,PopZ}}\cdot[\mathrm{PopZ_m}] - k_{\mathrm{aut,PopZ}}\cdot\left(1+\alpha_{\mathrm{PopZPodJ}}\cdot[\mathrm{PodJ}]_{\mathrm{T}}\right)\cdot[\mathrm{PopZ_m}]\cdot\left[\mathrm{PopZ_p}\right]^2 + k_{\mathrm{depol,PopZ}}\cdot\left[\mathrm{PopZ_p}\right] + D_{\mathrm{PopZm}}\cdot\frac{\partial^2[\mathrm{PopZ_m}]}{\partial x^2} \quad (1\text{-}4)$$

$$\frac{d[\mathrm{PopZ_p}]}{dt} = -\left(k_{\mathrm{d,PopZ}} + \mu\right)\cdot\left[\mathrm{PopZ_p}\right] + k_{\mathrm{dnv,PopZ}}\cdot[\mathrm{PopZ_m}] + k_{\mathrm{aut,PopZ}}\cdot\left(1+\alpha_{\mathrm{PopZPodJ}}\cdot[\mathrm{PodJ}]_{\mathrm{T}}\right)\cdot[\mathrm{PopZ_m}]\cdot\left[\mathrm{PopZ_p}\right]^2 - k_{\mathrm{depol,PopZ}}\cdot\left[\mathrm{PopZ_p}\right] + D_{\mathrm{PopZp}}\cdot\frac{\partial^2[\mathrm{PopZ_p}]}{\partial x^2} \quad (5\text{-}8)$$

where $k_{s,PopZ}$ and $k_{d,PopZ}$ indicate the synthesis rate and degradation rate of PopZ. μ is the growth rate of *Caulobacter* cell. $k_{dnv,PopZ}$ and $k_{aut,PopZ}$ represent the de novo polarization and autocatalytic polymer formation from PopZ monomer, respectively. $\alpha_{PopZPodJ}$ describes the nucleating function of PodJ on PopZ, which contributes to a stable bipolar pattern of PopZ. $k_{depol,PopZ}$ is the depolarization rate of PopZ. D_{PopZm} and D_{PopZp} are diffusion rates of monomer and polymer of PopZ respectively, where $D_{PopZp} \ll D_{PopZm}$. We use square brackets to represent concentrations.

Heterologous expression of PodJ alone in *E. coli* shows bipolar accumulation same as PopZ, which suggests that PodJ itself has high affinity of two poles [32]. why does PodJ specifically localize at new pole rather than two poles in *C. crescentus*? Zhao *et al* [32] has observed that PodJ accumulates at two poles in Δ*spmX Caulobacter* strain, while the accumulation of PodJ significantly reduces in the strain of overexpressed SpmX. Moreover, Co-expression of SpmX and PodJ in *E. coli* shows dispersed PodJ [32]. These observations suggest that SpmX directly inhibits PodJ assembly. Therefore, the inhibitory factor SpmX, which localizes at old pole of *C. crescentus*, likely causes the monopolar pattern of PodJ. Therefore, we integrate SpmX inhibition into the Turing model of $PodJ_L$ polymer (product) and monomer (substrate) to simulate the monopolar localization of PodJ as follows:

$$\frac{d[\mathrm{PodJ_{L,m}}]}{dt} = k_{\mathrm{s,PodJ}}\cdot\left((1-m)\cdot S_{\mathrm{PodJ}} + m\right) + k_{\mathrm{s,PodJ2}}\cdot\frac{J^4_{\mathrm{i,PodJCtrA}}}{J^4_{\mathrm{i,PodJCtrA}}+[\mathrm{CtrA\sim P}]^4} - \left(k_{\mathrm{d,PodJ1}} + k_{\mathrm{d,PodJ2}}\cdot[\mathrm{PerP}] + \mu\right)\cdot\left[\mathrm{PodJ_{L,m}}\right] - \frac{k_{\mathrm{dnv,PodJ}}}{1+\alpha_{\mathrm{PodJSpmX}}\cdot[\mathrm{SpmX_T}]}\cdot\left[\mathrm{PodJ_{L,m}}\right] - k_{\mathrm{aut,PodJ}}\cdot\left[\mathrm{PodJ_{L,m}}\right]\cdot\left[\mathrm{PodJ_{L,p}}\right]^2 + k_{\mathrm{depol,PodJ}}\cdot\left[\mathrm{PodJ_{L,p}}\right] + D_{\mathrm{PodJ,m}}\cdot\frac{\partial^2[\mathrm{PodJ_{L,m}}]}{\partial x^2} \quad (9\text{-}12)$$

$$\frac{d[\mathrm{PodJ_{L,p}}]}{dt} = -\left(k_{\mathrm{d,PodJ1}} + k_{\mathrm{d,PodJ2}}\cdot[\mathrm{PerP}] + \mu\right)\cdot[\mathrm{PodJ_{L,p}}] + \frac{k_{\mathrm{dnv,PodJ}}}{1+\alpha_{\mathrm{PodJSpmX}}\cdot[\mathrm{SpmX_T}]}\cdot\left[\mathrm{PodJ_{L,m}}\right] + k_{\mathrm{aut,PodJ}}\cdot\left[\mathrm{PodJ_{L,m}}\right]\cdot\left[\mathrm{PodJ_{L,p}}\right]^2 - k_{\mathrm{depol,PodJ}}\cdot\left[\mathrm{PodJ_{L,p}}\right] + D_{\mathrm{PodJ,p}}\cdot\frac{\partial^2[\mathrm{PodJ_{L,p}}]}{\partial x^2} \quad (13\text{-}16)$$

where $((1-m)S_{PodJ}+m)$ describes the methylation regulation of PodJ expression (explained in section 2.4). $J_{i,PodJCtrA}$ indicates the binding affinity between CtrA~P and *podJ* promoter, which is involved in the term representing CtrA~P suppression of *podJ*

expression. In equations, italics represents gene or mRNA, while non-italic species indicates protein.

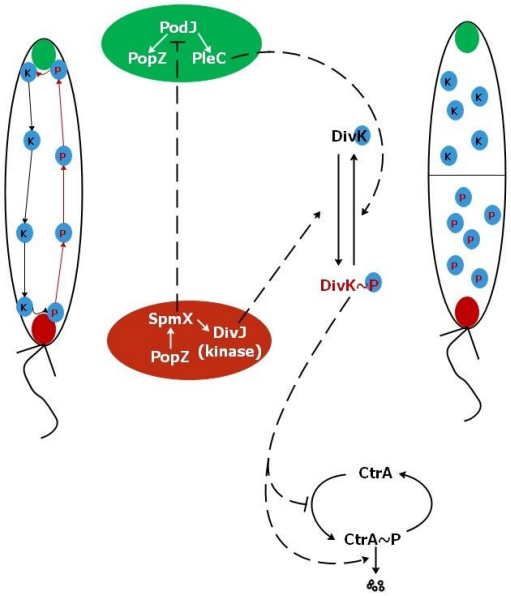

Figure 3. Schematic model of polarity and asymmetry establishment. The new pole and old pole are indicated as green and red ellipses, respectively. White line indicates positive recruitment effect. Dash line indicates activation using arrows and inhibition using bar. Conversion between phosphorylated and unphosphorylated DivK is regulated by DivJ and PleC. DivK~P inhibits phosphorylation of CtrA and promotes the proteolysis of CtrA.

2.3 Spatial Gradient of Phosphorylated CtrA

Phosphorylated CtrA is the active form that plays essential roles in controlling DNA replication initiation and transcriptions. CtrA~P is rich in swarmer cells and cleared during the sw-to-st transition (Fig. 1, nude). Spatial gradient of CtrA~P is formed before cytokinesis, which results in daughter swarmer cell with rich CtrA~P and daughter stalked cell with little CtrA~P [4]. The non-uniform distributed CtrA~P is the essential determinant of different fates of progenies [30]. The activity of CtrA is regulated by phosphorylation and abundance. While the localization mechanism of CtrA proteolysis is yet fully understood, spatial localization of CtrA phosphorylation has been recently elucidated [4,26,29].

CckA is the only known phosphoryl source of CtrA, the kinase activity of which is inhibited by DivK [31]. DivK also shows spatial gradient during cell cycle, which is mainly regulated by the kinase DivJ and phosphatase PleC [29]. PleC is recruited by the new polar PodJ, while DivJ is recruited by SpmX at the old pole [32]. Additionally, SpmX does not only influence the localization but also the activity of DivJ [24]. Therefore, we can connect scaffolding proteins with protein phosphorylation.

Due to the direct and indirect recruitment by scaffolding proteins PodJ and PopZ, SpmX and DivJ are mainly located at old poles (Fig. 1, lavender, and orange), while most PleC proteins localize at new poles (Fig. 1, green). We use PopZ as a nucleating factor of SpmX (Eq.21-28) and introduce free DivJ/PleC as well as bound DivJ/PleC based on their spatial organization (Eq.37-52). Unphosphorylated DivK diffuse in swarmer cells, while DivK~P occupies the old pole of *C. crescentus* after the sw-to-st transition (Fig.1, pink and red). DivK~P produces a second focus at the new pole later and is released from the new pole with the completion of cytokinesis (Fig. 1, red). As there is a positive correlation between phosphorylation and localization of DivK, we introduce two forms of DivK~P, $DivKP_f$ and $DivKP_b$, into our system to model this characteristic (Eq. 57-64). Therefore, DivJ and PleC, which localize at opposite poles and regulate DivK phosphorylation, should play key roles in the spatial distribution of DivK.

In this work, we proposed a simplified network (Fig. 3) to investigate the spatial gradient of master regulator CtrA in *C. crescentus* with following assumptions:

a). Although PleC is bifunctional with both kinase and phosphatase activities, it is the principal phosphatase but minor kinase of DivK and PleD in *C. crescentus* [23]. In this simplified model, we only considered the phosphatase activity of PleC.

b). As mentioned previously, PodJ shows high affinity with poles. The candidate mechanisms are nucleoid occlusion and specific recognition of unique curvature or peptidoglycan composition of cell poles [12]. As there is no ensured mechanism of polarly localization for PodJ, we assume $k_{aut,PodJ}$ in polar compartments is higher than those in central compartments to highlight the specific affinity of poles.

c). Only bound DivJ is active in our model because SpmX regulates DivJ activity.

d). mRNAs of *C. crescentus* have a low diffusion rate ($\approx 0.03 \mu m^2/min$), which implies a spatial synthesis of proteins [20]. Therefore, we assumed that the synthesis of involved proteins only take place in central compartments due to the position of corresponding genes [8] (Fig. 4). We let $k_{s,*}=0$ in polar compartments (Eq. 1, 4, 9, 12, 21, 24, 29, 32, 37, 40, 45, 48, 53, 56).

e). In order to effectively model mechanisms underlying asymmetry established by spatially organized scaffolding proteins, we ignore the phosphorylation mediator CckA and proteolysis mediator CpdR of CtrA; and assume DivK directly controls the phosphorylation and proteolysis of CtrA in our model (Fig. 3).

ODEs except for PopZ and $PodJ_L$ (Eq. 1-16) are listed in Table 1. Parameters and initial values are listed in Table 2 and 3.

2.4 Check Points in Cell Cycle

DnaA, which is essential for DNA replication initiation, is not involved in this model because DnaA is not closely related with asymmetry formation. We take a low threshold of CtrA~P level as a synchronous event of DNA replication initiation and record the time of as T_{ini} (Table 4) [21]. The period of S-phase is approximately 90 min [10]. Therefore, we set replication termination time (Table 4, T_{term}) as T_{ini}+90 min. Promoters of *ctrA*, *pleC*, *perP*, and *podJ* are regulated by methylation [15]. As

we do not include the methyltransferase CcrM, we use (1-m)S+m (Table 1) to represent the methylation status of chromosome as follows:

- S=0: fully-methylated chromosome
- S=1: hemi-methylated chromosome

where m is a small number indicating the low expression of fully-methylated genes.

Based on genome coordinates of genes (Fig. 4), we can calculate the approximate time when replication fork passes the corresponding gene. When the replication fork passes the gene, S is set to 1. All events are listed in Table 4.

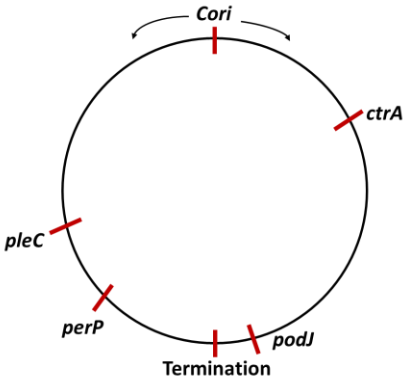

Figure 4. Genomic coordinates of *C. crescentus*. Replication forks bidirectionally move from *Cori* to the termination area (arrows). *ctrA*, *pleC*, *perP*, and *podJ* approximately localize at 37%, 65%, 74% and 87% of the half chromosome [15]. Based on DNA replication initiation time (T_{ini}) and termination time (T_{term}), the time when forks pass corresponding gene can be calculated.

3 Results

In order to verify our model and explore the parameter space, we simulate our mathematical model for five cell cycles and compare the simulated results with reported experimental measurement in literature.

In the following we mainly show results of the third cycle (if not specified) for illustrations. All simulations are done through MATLAB.

3.1 Spatial simulation in swarmer and stalked cell

Figure 5 shows spatial dynamics of $PodJ_L$, $PodJ_S$, PopZ, SpmX, PleC, DivJ, DivK~P, and CtrA~P in the swarmer cell simulation. Our four-compartment method divides the entire cell into 4 bins, where the top bin and bottom bin in Figure 5 indicate the new pole and old pole, respectively. Compared with experimental observations summarized in Figure 1, our model correctly captures the spatial dynamics of most proteins except the temporary accumulation of DivK~P at the new pole.

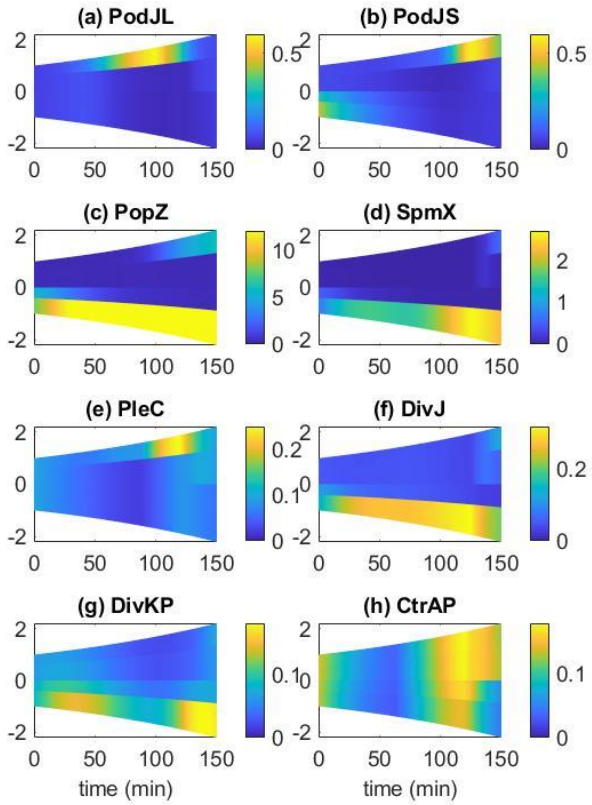

Figure 5. Heatmaps of 4-compartment spatial simulation over one replication cycle of *Caulobacter* swarmer cell. Y-axis indicates distance to midpoint, representing position of compartment. Top compartment represents the new pole while bottom compartment represents the old pole. Color of heatmap indicates scaled concentration in each compartment.

Our simulated long form PodJ occupies the new pole and is degraded in the late predivional cell (Fig. 5a), which is consistent with experiments (Fig. 1, dark blue). The stable monopolar localization of $PodJ_L$ is ensured by the higher autocatalytic polymerization in polar compartments and the dispersion effect of SpmX. The short form PodJ in simulation (Fig. 5b) is degraded from the old pole during the sw-to-st transition, reappears at the new pole in the late predivisional cell, and is inherited by the nascent swarmer cell. $PodJ_S$ simulation agrees with observations [32]. PopZ simulation is stably bipolar (Fig. 5c), which is consistent with experiments. In details, PopZ initiates to present at the new pole around 50 min while rapidly accumulates at new pole around 90 min in simulation. Experiment indicates wild type PopZ stably accumulates at the new pole at approximately 60 min, which is earlier than our simulation [32]. SpmX occupies the old pole throughout the cell cycle, which agrees with experimental observations (Fig. 5d). The synthesis taking place only in central compartments weakens the polar localization of Turing pattern proteins (data not shown), but our system is sufficiently robust to generate polarly distribution for PodJ, PopZ, and SpmX.

Kinase DivJ is recruited by SpmX and shows stable accumulation at the old pole in our simulation (Fig. 5f). Simulated PleC is consistent with observations as well: most of PleC are located at the new pole (Fig. 5e). Most of DivK~P localize at the old pole, consistent with experiments (Fig. 5g). However, we expect a temporary accumulation of DivK~P at the new pole in the early predivional cell, but our simulation does not have this behavior. The discrepancy is likely because we only include phosphatase activity of PleC in this preliminary model rather than considering the kinase activity of PleC. Therefore, DivK~P cannot present at new pole due to the stable active phosphatase. The CtrA dynamics in our simulation fits experimental observations very well (Fig. 5h), which is cleared during the sw-to-st transition and in the stalked compartment. The nascent swarmer cell is rich of CtrA~P [30]. Our model suggests that the nonuniform distribution of kinase and phosphatase is sufficient for CtrA spatial gradient and asymmetric inheritance of distinct daughter cells.

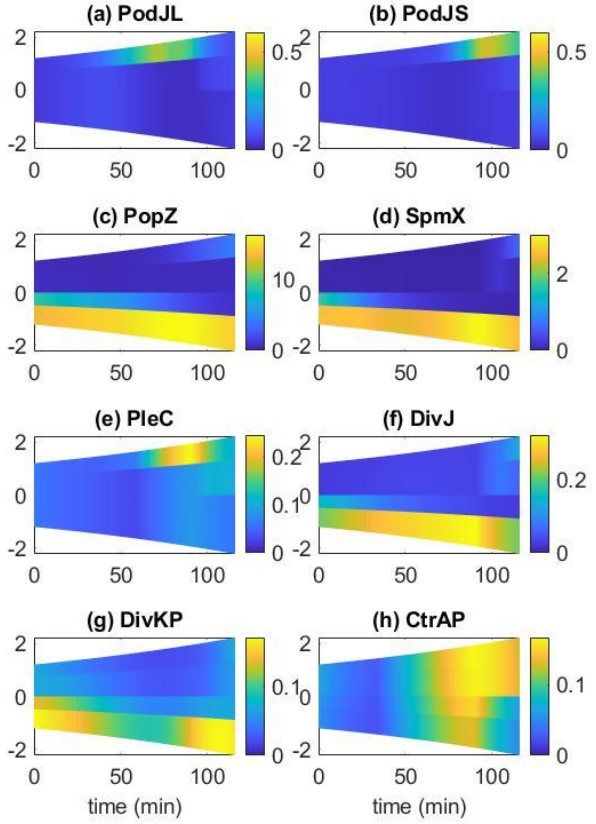

Figure 6. Heatmaps of 4-compartment spatial simulation over one replication cycle of *Caulobacter* stalked cell.

Spatial simulation of stalked cell cycle is shown in Fig. 6. Although there is no experiment monitoring spatial dynamics in stalked cell, we can use the observations of swarmer cell after 30 min to approximately assess our simulation. The three essential proteins of polarity establishment, PodJ, PopZ, and SpmX, are localized at correct polar areas (Fig. 6, a-d). Additionally, DivK~P and CtrA~P exhibit reasonable gradient in simulation (Fig. 6, g and h).

3.2 Levels of two types of PodJ over cell cycle

Compared with the temporal dynamics from Chen *et al* and Guo *et al* [3,6], our simulated temporal $PodJ_L$ and $PodJ_S$ have similar features over cell cycles, though $PodJ_L$ at the beginning is a little higher than experiments (Fig. 7). $PodJ_L$ is synthesized while $PodJ_S$ is degraded at the early stage of cell cycle. The reducing trend of $PodJ_S$ continues until the replication fork passes *perP*, which encodes the protease PerP truncating $PodJ_L$ to $PodJ_S$. The inconsistence at the beginning of cycle may come from the expression of PerP, which may end early in our simulation, resulting in higher $PodJ_L$ level. As we do not simulate Z-ring constriction and cell division process in this work, the estimated time of DNA replication termination likely results in this imprecise simulation. Another candidate cause is experimental errors because the level of $PodJ_L$ may be too low to accurately measure.

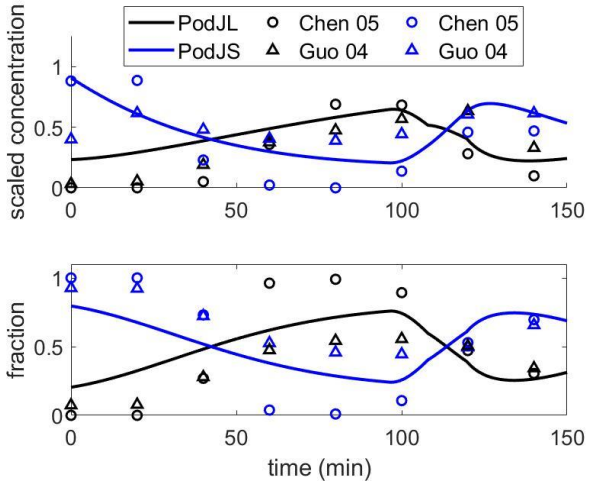

Figure 7. Temporal dynamics of concentration and fraction of $PodJ_L$ and $PodJ_S$ in swarmer cell. $PodJ_L$ level is lower than $PodJ_S$ at the beginning of cell cycle. $PodJ_S$ then is proteolyzed while $PodJ_L$ is newly synthesized during sw-to-st transition. PerP works in the late predivisional cell to truncate $PodJ_L$ to $PodJ_S$.

3.3 PodJ is required for stable bipolar PopZ and localized PleC

We investigate the distribution of PopZ, PleC, and SpmX in Δ*podJ in silico* (Fig. 8, left-third cycle; right-forth cycle). Without recruitment by PodJ, PleC is dispersed throughout the cell, which agrees with experimental observations [32]. Most PopZ accumulates at one pole in Δ*podJ* rather than stably generates a second focus at the opposite pole. Our simulation shows that PopZ switches to localize at different poles, with a faded second focus when localizing at new poles in Δ*podJ* (Fig. 8). PopZ localizes at old poles in the first, third, and fifth cycle and mainly at new poles in the second and forth cycle. Experimental observations verify that newly synthesized PopZ localizes at the old pole in most *C. crescentus* cell (91%) and only 9% of samples show a new polar accumulation of PopZ in Δ*podJ* [32]. As our

current model is a deterministic model, we cannot capture the fraction of simulations with specific characteristics. However, our model does suggest that the bipolar pattern of PopZ significantly depends on PodJ. As SpmX is recruited by PopZ, our model suggests SpmX co-localizes with PopZ in Δ*podJ*.

We also check the spatial dynamics of PopZ and PleC in *podJ*+, of which $k_{s,podJ}$ increases to 2-fold of wild type strain in simulation (Fig. 9). Our model suggests overexpression of PodJ results in a stronger and earlier accumulation at the new pole for both PopZ and PleC. Our simulation of PopZ in *podJ*+ resembles experimental data where PopZ quickly generates a new focus of new pole at around t=50min [32].

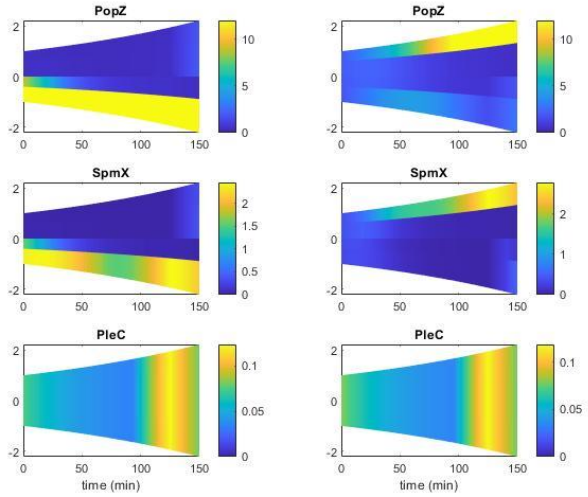

Figure 8. Simulated spatial dynamics in Δ*podJ* strain. Left column is the third simulated cycle, while right column is the fourth simulated cycle. PopZ switches to localize at opposite poles. SpmX co-localizes with PopZ. PleC is uniformly distributed throughout the cell in Δ*podJ* strain.

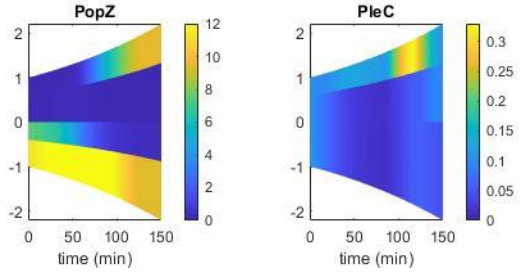

Figure 9. Simulated spatial dynamics in *podJ*+ strain. Compared with wild type, both PopZ and PleC show stronger and earlier accumulation at the new pole.

Discussion

In this work, we construct a scaffolding proteins network as the foundation of polarity establishment in *C. crescentus*. PodJ and PopZ work as scaffolding proteins recruiting key kinase and phosphatase at opposite poles and promote the spatial gradient of regulators DivK and CtrA. The non-uniformly distribution of client proteins determine different fates of newborn daughter cells, where swarmer cell is motile and non-replicable and stalked cell is sessile and replicable. Our spatiotemporal model successfully captures key features of both scaffolding and client proteins in space and time. Our wild type and mutant strains simulation suggest that PodJ is sufficient and required for the bipolar pattern of PopZ. A higher affinity of poles is necessary for polar accumulation of PodJ (data not shown), which derives from the attribute of Turing pattern favoring central assembly. In Δ*podJ* simulation, we found a biased affinity of poles is also required for the polarly distribution of PopZ (data not shown) because PopZ still localizes at one pole when there is no asymmetric attraction from PodJ in Δ*podJ*. Therefore, our model suggests that there should be unknown mechanisms independent of PodJ resulting in higher affinity of poles for PopZ.

Our simulations are in good agreement with experimental observations. However, there are still interesting future directions that we will extend:

1). Our four-compartment can capture the dynamics of poles, central area, and midcell, efficiently and separately. However, the simple method may reduce the accuracy of simulation. Therefore, we will extend our four-compartment model to a more precise model in the future, with more compartments.

2). The kinase activity of PleC will be introduced into the system.

3). The indirect regulation between DivK and CtrA is simplified by a direct connection in the current model. We will introduce intermediate regulators, DivL and CckA, into the spatial regulatory network to improve the accuracy. Additionally, CtrA proteolysis in space should receive more attentions.

4). Z-ring constriction controlled by FtsZ will be introduced to accurately simulate the cell division and separation time.

ACKNOWLEDGMENTS

This work was partially supported by the National Science Foundation (NSF) under awards MCB-1613741, and CCF-1909122.

Table 1. ODEs of the four-compartment model

$\frac{d[\mathrm{PodJ_s}]}{dt} = \left(k_{\mathrm{d,PodJ1}} + k_{\mathrm{d,PodJ2}} \cdot [\mathrm{PerP}]\right) \cdot \left([\mathrm{PodJ_{L,m}}] + [\mathrm{PodJ_{L,p}}]\right) - (\mu + k_{\mathrm{d,PodJS}}) \cdot [\mathrm{PodJ_s}]$ (17-20)
$\frac{d[\mathrm{SpmX_m}]}{dt} = k_{\mathrm{s,SpmX}} \cdot \frac{[\mathrm{CtrA{\sim}P}]^2}{[\mathrm{CtrA{\sim}P}]^2 + J_{\mathrm{a,SpmXCtrA}}{}^2} - \left(k_{\mathrm{d,SpmX}} + \mu\right) \cdot [\mathrm{SpmX_m}] - k_{\mathrm{dnv,SpmX}} \cdot [\mathrm{SpmX_m}] - k_{\mathrm{aut,SpmX}} \cdot (1 + \alpha_{\mathrm{SpmXPopZ}} \cdot [\mathrm{PopZ_T}]) \cdot [\mathrm{SpmX_m}] \cdot [\mathrm{SpmX_p}]^2 + k_{\mathrm{depol,SpmX}} \cdot [\mathrm{SpmX_p}] + D_{\mathrm{SpmX,m}} \cdot \frac{\partial^2 [\mathrm{SpmX_m}]}{\partial x^2}$ (21-24)
$\frac{d[\mathrm{SpmX_p}]}{dt} = -\left(k_{\mathrm{d,SpmX}} + \mu\right) \cdot [\mathrm{SpmX_p}] + k_{\mathrm{dnv,SpmX}} \cdot [\mathrm{SpmX_m}] + k_{\mathrm{aut,SpmX}} \cdot (1 + \alpha_{\mathrm{SpmXPopZ}} \cdot [\mathrm{PopZ_T}]) \cdot [\mathrm{SpmX_m}] \cdot [\mathrm{SpmX_p}]^2 - k_{\mathrm{depol,SpmX}} \cdot [\mathrm{SpmX_p}] + D_{\mathrm{SpmX,p}} \cdot \frac{\partial^2 [\mathrm{SpmX_p}]}{\partial x^2}$ (25-28)
$\frac{d[\mathrm{CtrA}]}{dt} = k_{\mathrm{s,CtrA1}} \cdot \left(1 - \frac{[\mathrm{CtrA{\sim}P}]}{J_{\mathrm{i,CtrACtrA}} + [\mathrm{CtrA}] + [\mathrm{CtrA{\sim}P}]}\right) \cdot \left((1-m) \cdot S_{\mathrm{CtrA}} + m\right) + k_{\mathrm{s,CtrA2}} \cdot \frac{[\mathrm{CtrA{\sim}P}]}{J_{\mathrm{a,CtrACtrA}} + [\mathrm{CtrA}] + [\mathrm{CtrA{\sim}P}]} - (\mu + k_{\mathrm{d,CtrA1}} + k_{\mathrm{d,CtrA2}} \cdot$

$$\frac{[\text{DivK}\sim\text{P}]_T^2}{J_{d,\text{CtrA}}{}^2+[\text{DivK}\sim\text{P}]_T^2}) \cdot [\text{CtrA}] - k_{\text{phoCtrA}} \cdot [\text{CtrA}] + k_{\text{dephoCtrA}} \cdot [\text{DivK}\sim\text{P}]_T \cdot [\text{CtrA}\sim\text{P}] + D_{\text{CtrA}} \cdot \frac{\partial^2[\text{CtrA}]}{\partial x^2} \quad (29\text{-}32)$$

$$\frac{d[\text{CtrA}\sim\text{P}]}{dt} = -\left(\mu + k_{\text{d,CtrA1}} + k_{\text{d,CtrA2}} \cdot \frac{[\text{DivK}\sim\text{P}]_T^2}{J_{\text{d,CtrA}}{}^2+[\text{DivK}\sim\text{P}]_T^2}\right) \cdot [\text{CtrA}\sim\text{P}] + k_{\text{phoCtrA}} \cdot [\text{CtrA}] - k_{\text{dephoCtrA}} \cdot [\text{DivK}\sim\text{P}]_T \cdot [\text{CtrA}\sim\text{P}] + D_{\text{CtrA}} \cdot \frac{\partial^2[\text{CtrA}\sim\text{P}]}{\partial x^2} \quad (33\text{-}36)$$

$$\frac{d[\text{PleC}]_f}{dt} = k_{\text{s,PleC}} \cdot ((1-m_{\text{pleC}}) \cdot S_{\text{PleC}} + m_{\text{pleC}}) - \left(\mu + k_{\text{d,PleC}}\right) \cdot [\text{PleC}]_f - k_{\text{fb-PleC}} \cdot (1 + \alpha_{\text{PleCPodJ}} \cdot [\text{PodJ}]_T) \cdot [\text{PleC}]_f + k_{\text{bf-PleC}} \cdot [\text{PleC}]_b + D_{\text{PleC}} \cdot \frac{\partial^2[\text{PleC}]_f}{\partial x^2} \quad (37\text{-}40)$$

$$\frac{d[\text{PleC}]_b}{dt} = -\left(\mu + k_{\text{d,PleC}}\right) \cdot [\text{PleC}]_b + k_{\text{fb-PleC}} \cdot (1 + \alpha_{\text{PleCPodJ}} \cdot [\text{PodJ}]_T) \cdot [\text{PleC}]_f - k_{\text{bf-PleC}} \cdot [\text{PleC}]_b \quad (41\text{-}44)$$

$$\frac{d[\text{DivJ}]_f}{dt} = k_{\text{s,DivJ}} - \left(\mu + k_{\text{d,DivJ}}\right) \cdot [\text{DivJ}]_f - k_{\text{fb-DivJ}} \cdot (1 + \alpha_{\text{DivJSpmX}} \cdot [\text{SpmX}]_T) \cdot [\text{DivJ}]_f + k_{\text{bf-DivJ}} \cdot [\text{DivJ}]_b + D_{\text{DivJ}} \cdot \frac{\partial^2[\text{DivJ}]_b}{\partial x^2} \quad (45\text{-}48)$$

$$\frac{d[\text{DivJ}]_b}{dt} = -\left(\mu + k_{\text{d,DivJ}}\right) \cdot [\text{DivJ}]_b + k_{\text{fb-DivJ}} \cdot (1 + \alpha_{\text{DivJSpmX}} \cdot [\text{SpmX}]_T) \cdot [\text{DivJ}]_f - k_{\text{bf-DivJ}} \cdot [\text{DivJ}]_b \quad (49\text{-}52)$$

$$\frac{d[\text{DivK}]}{dt} = k_{\text{s,DivK1}} + k_{\text{s,DivK2}} \cdot \frac{[\text{CtrA}\sim\text{P}]^2}{J_{\text{a,DivKCtrA}}{}^2+[\text{CtrA}\sim\text{P}]^2} - \left(\mu + k_{\text{d,DivK}}\right) \cdot [\text{DivK}] - k_{\text{phoDivK}} \cdot (1 + \alpha_{\text{DivKDivJ}} \cdot [\text{DivJ}]_b) \cdot [\text{DivK}] + k_{\text{dephoDivK}} \cdot [\text{PleC}] \cdot [\text{DivK}\sim\text{P}]_T + D_{\text{DivK}} \cdot \frac{\partial^2[\text{DivK}]}{\partial x^2} \quad (53\text{-}56)$$

$$\frac{d[\text{DivK}\sim\text{P}]_f}{dt} = -\left(\mu + k_{\text{d,DivK}}\right) \cdot [\text{DivK}\sim\text{P}]_f + k_{\text{phoDivK}} \cdot \left(1 + \alpha_{\text{DivKDivJ}} \cdot [\text{DivJ}]_b\right) \cdot [\text{DivK}] - k_{\text{dephoDivK}} \cdot [\text{PleC}] \cdot [\text{DivK}\sim\text{P}]_f - k_{\text{fb-DivKP}} \cdot [\text{DivK}\sim\text{P}]_f + k_{\text{bf-DivKP}} \cdot [\text{DivK}\sim\text{P}]_b + D_{\text{DivK}} \cdot \frac{\partial^2[\text{DivK}\sim\text{P}]_f}{\partial x^2} \quad (57\text{-}60)$$

$$\frac{d[\text{DivK}\sim\text{P}]_b}{dt} = -\left(\mu + k_{\text{d,DivK}}\right) \cdot [\text{DivK}\sim\text{P}]_b + k_{\text{fb-DivKP}} \cdot [\text{DivK}\sim\text{P}]_f - k_{\text{bf-DivKP}} \cdot [\text{DivK}\sim\text{P}]_b \quad (61\text{-}64)$$

$$\frac{d[\text{PerP}]}{dt} = k_{\text{s,PerP}} \cdot \frac{[\text{CtrA}\sim\text{P}]^2}{[\text{CtrA}\sim\text{P}]^2+J_{\text{a,PerPCtrA}}{}^2} \cdot ((1-m) \cdot S_{\text{PerP}} + m) - (\mu + k_{\text{d,PerP}}) \cdot [\text{PerP}] + D_{\text{PerP}} \cdot \frac{\partial^2[\text{PerP}]}{\partial x^2} \quad (65\text{-}68)$$

Table 2. parameters

$k_{s,PopZ}$=0.15μM/min	$k_{d,PopZ}$=0.01μM/min	$k_{dnv,PopZ}$=42/min
$k_{aut,PopZ}$(polar)=12μM^{-2}min^{-1}	$k_{aut,PopZ}$(central)=8.4μM^{-2}min^{-1}	$D_{PopZ,m}$=835μm^2/min [13]
$k_{depol,PopZ}$=0.05/min	μ=0.0053/min [2]	$\alpha_{PopZPodJ}$=50
$D_{PopZ,p}$=0.0005μm^2/min	m=0.01	$k_{s,PodJ}$=0.01μM/min
$k_{s,PodJ2}$=0.006 μM/min	$J_{i,PodJCtrA}$=0.5μM	$k_{d,PodJ1}$=0.007μM/min
$k_{d,PodJ2}$=0.3μM/min	$k_{dnv,PodJ}$=1.5/min	$\alpha_{PodJSpmX}$=200
$k_{aut,PodJ}$(polar)=300μM^{-2}min^{-1}	$k_{aut,PodJ}$(central)=0μM^{-2}min^{-1}	$k_{depol,PodJ}$=0.1/min
$D_{PodJ,m}$=100μm^2/min [13]	$D_{PodJ,p}$=.0005μm^2/min	$k_{d,PodJS}$=0.025/min
$k_{s,SpmX}$=0.24μM/min	$J_{a,SpmXCtrA}$=1μM	$k_{d,SpmX}$=0.01/min
$k_{dnv,SpmX}$=0.1/min	$\alpha_{SpmXPopZ}$=50	$k_{depol,SpmX}$=0.036/min
$k_{aut,SpmX}$=0.1μM^{-2}min^{-1}	$D_{SpmX,m}$=200μm^2/min [13]	$D_{SpmX,}$p=0.0005μm^2/min
$k_{s,CtrA1}$=0.008 μM/min	$J_{i,CtrACtrA}$=3μM	$k_{s,CtrA2}$=0.073μM/min
$J_{a,CtrACtrA}$=3μM	$k_{d,CtrA1}$=0.0038/min [5]	$k_{d,CtrA2}$=0.15/min
$J_{d,CtrA}$=0.2μM	$k_{pho,CtrA}$=3e^{3}μM^{-1}min^{-1} [4]	$k_{depho,CtrA}$=8.66e^{3}μM^{-1}min^{-1} [4]
D_{CtrA}=427μm^2/min [13]	$k_{s,PleC}$=0.01μM/min	m_{PleC}=0.15
$k_{d,PleC}$=0.02/min	$k_{fb-PleC}$=1μM^{-1}min^{-1}	$k_{bf-PleC}$=0.5μM^{-1}min^{-1}
$\alpha_{PleCPodJ}$=10	D_{PleC}=71μm^2/min [13]	$k_{s,DivJ}$=0.016μM/min
$k_{d,DivJ}$=0.07/min	$k_{fb-DivJ}$=1μM^{-1}min^{-1}	$k_{bf-DivJ}$=0.5μM^{-1}min^{-1}
$\alpha_{DivJSpmX}$=5	D_{DivJ}=108μm^2/min [13]	$k_{s,DivK1}$=0.0004μM/min
$J_{a,DivKCtrA}$=0.7μM	$k_{s,DivK2}$=0.15μM/min	$k_{d,DivK}$=0.052/min
$k_{pho,DivK}$=0.01μM^{-1}min^{-1}	$\alpha_{DivKDivJ}$=50	$k_{depho,DivK}$=101μM^{-1}min^{-1}
D_{DivK}=1319μm^2/min [13]	$k_{fb-DivKP}$=10000/min	$k_{bf-DivKP}$=0.1/min
$k_{s,PerP}$=0.5μM/min	$J_{a,PerPCtrA}$=0.5μM	$k_{d,PerP}$=0.04/min
D_{PerP}=853μm^2/min [13]		

Table 3. Initial Value

$PodJ_m$=0μM	$PodJ_{L,p}$=1e^{-5}μM	$PodJ_S$=1μM(old pole)
$PodJ_S$=1e^{-3}μM	$SpmX_m$=0μM	$SpmX_p$=0μM
$PopZ_m$=0μM	$PopZ_p$=2μM(old pole)	$PopZ_p$=0.5μM
CtrA=0.2μM	CtrA~P=0.5μM	$PleC_f$=0.05μM
$PleC_b$=0.05μM(pole)	$PleC_b$=0μM	$DivJ_f$=0μM
$DivJ_b$=0μM	DivK=0.2μM	DivK~P_f=0μM
DivK~P_b=0μM	$l_{1,4}$=0.4μm	$l_{2,3}$=0.6μm

Table 4. Event of the spatial model

Event description	condition	change at the event
Replication Initiation	[CtrA~P]<threshold(=0.25)	T_{ini}=t
Replication fork passes *ctrA*	t>90*37%+T_{ini}	$S_{CtrA} = 1$
Replication fork passes *pleC*	t>90*65%+ T_{ini}	$S_{PleC} = 1$
Replication fork passes *perP*	t>90*74%+ T_{ini}	$S_{PerP} = 1$
Replication fork passes *podJ*	t>90*87%+ T_{ini}	$S_{PodJ} = 1$
Replication Termination	t>T_{term}	S = 0

REFERENCES

1. Nora Ausmees and Christine Jacobs-Wagner. 2003. Spatial and Temporal Control of Differentiation and Cell Cycle Progression in Caulobacter crescentus. *Annual Review of Microbiology* 57, 1: 225–247. https://doi.org/10.1146/annurev.micro.57.030502.091006

2. Manuel Campos, Ivan V Surovtsev, Setsu Kato, Ahmad Paintdakhi, Bruno Beltran, Sarah E Ebmeier, and Christine Jacobs-Wagner. 2014. A constant size extension drives bacterial cell size homeostasis. *Cell* 159, 6: 1433–1446.

3. Joseph C. Chen, Alison K. Hottes, Harley H. McAdams, Patrick T. McGrath, Patrick H. Viollier, and Lucy Shapiro. 2006. Cytokinesis signals truncation of the PodJ polarity factor by a cell cycle-regulated protease. *EMBO Journal* 25, 2: 377–386. https://doi.org/10.1038/sj.emboj.7600935

4. Y Erin Chen, Carolina Tropini, Kristina Jonas, Christos G Tsokos, Kerwyn C Huang, and Michael T Laub. 2011. Spatial gradient of protein phosphorylation underlies replicative asymmetry in a bacterium. *Proceedings of the National Academy of Sciences* 108, 3: 1052 LP – 1057. https://doi.org/10.1073/pnas.1015397108

5. Ibrahim J Domian, Kim C Quon, and Lucy Shapiro. 1997. Cell type-specific phosphorylation and proteolysis of a transcriptional regulator

controls the G1-to-S transition in a bacterial cell cycle. *Cell* 90, 3: 415–424.

6. Xiaoyun Guo. 2014. A bacterial scaffolding protein keeps the cell cycle and differentiation in check by regulating histidine kinase activity.

7. Kerwyn Casey Huang and Kumaran S Ramamurthi. 2010. Macromolecules that prefer their membranes curvy. *Molecular microbiology* 76, 4: 822–832.

8. Rasmus B Jensen, Sherry C Wang, and Lucy Shapiro. 2001. A moving DNA replication factory in Caulobacter crescentus. *The EMBO journal* 20, 17: 4952–4963.

9. Kamal Kishore Joshi, Christine M Battle, and Peter Chien. 2018. Polar localization hub protein PopZ restrains adaptor-dependent ClpXP proteolysis in Caulobacter crescentus. *Journal of bacteriology* 200, 20.

10. Kenneth C Keiler and Lucy Shapiro. 2003. tmRNA is required for correct timing of DNA replication in Caulobacter crescentus. *Journal of bacteriology* 185, 2: 573–580.

11. Shigeru Kondo and Takashi Miura. 2010. Reaction-diffusion model as a framework for understanding biological pattern formation. *science* 329, 5999: 1616–1620.

12. Kimberly Ann Kowallis. 2020. Regulatory Mechanisms of a Bacterial Multi-Kinase Network. UNIVERSITY OF PITTSBURGH. https://doi.org/10.4324/9781315776095-80

13. Mohit Kumar, Mario S Mommer, and Victor Sourjik. 2010. Mobility of cytoplasmic, membrane, and DNA-binding proteins in Escherichia coli. *Biophysical journal* 98, 4: 552–559.

14. Keren Lasker, Thomas H Mann, and Lucy Shapiro. 2016. An intracellular compass spatially coordinates cell cycle modules in Caulobacter crescentus. *Current Opinion in Microbiology* 33: 131–139. https://doi.org/https://doi.org/10.1016/j.mib.2016.06.007

15. Keren Lasker, Jared M Schrader, Yifei Men, Tyler Marshik, David L Dill, Harley H McAdams, and Lucy Shapiro. 2016. CauloBrowser: A systems biology resource for Caulobacter crescentus. *Nucleic Acids Research* 44, D1: D640–D645.

16. Michael T Laub, Swaine L Chen, Lucy Shapiro, and Harley H McAdams. 2002. Genes directly controlled by CtrA, a master regulator of the Caulobacter cell cycle. *Proceedings of the National Academy of Sciences* 99, 7: 4632–4637.

17. Melanie L Lawler, David E Larson, Aaron J Hinz, David Klein, and Yves V Brun. 2006. Dissection of functional domains of the polar localization factor PodJ in Caulobacter crescentus. *Molecular microbiology* 59, 1: 301–316.

18. Shenghua Li, Paul Brazhnik, Bruno Sobral, and John J Tyson. 2008. A quantitative study of the division cycle of Caulobacter crescentus stalked cells. *PLoS computational biology* 4, 1.

19. Shenghua Li, Paul Brazhnik, Bruno Sobral, and John J Tyson. 2009. Temporal controls of the asymmetric cell division cycle in Caulobacter crescentus. *PLoS computational biology* 5, 8: e1000463–e1000463. https://doi.org/10.1371/journal.pcbi.1000463

20. Paula Montero Llopis, Audrey F Jackson, Oleksii Sliusarenko, Ivan Surovtsev, Jennifer Heinritz, Thierry Emonet, and Christine Jacobs-Wagner. 2010. Spatial organization of the flow of genetic information in bacteria. *Nature* 466, 7302: 77–81.

21. Seán M Murray, Gaël Panis, Coralie Fumeaux, Patrick H Viollier, and Martin Howard. 2013. Computational and genetic reduction of a cell cycle to its simplest, primordial components. *PLoS Biol* 11, 12: e1001749.

22. Adam M Perez, Thomas H Mann, Keren Lasker, Daniel G Ahrens, Michael R Eckart, and Lucy Shapiro. 2017. A localized complex of two protein oligomers controls the orientation of cell polarity. *MBio* 8, 1.

23. Francesco Pini, Benjamin Frage, Lorenzo Ferri, Nicole J De Nisco, Saswat S Mohapatra, Lucilla Taddei, Antonella Fioravanti, Frederique Dewitte, Marco Galardini, and Matteo Brilli. 2013. The DivJ, CbrA and PleC system controls DivK phosphorylation and symbiosis in S inorhizobium meliloti. *Molecular microbiology* 90, 1: 54–71.

24. Sunish Kumar Radhakrishnan, Martin Thanbichler, and Patrick H Viollier. 2008. The dynamic interplay between a cell fate determinant and a lysozyme homolog drives the asymmetric division cycle of Caulobacter crescentus. *Genes & development* 22, 2: 212–225.

25. Lars D Renner and Douglas B Weibel. 2012. MinD and MinE interact with anionic phospholipids and regulate division plane formation in Escherichia coli. *Journal of Biological Chemistry* 287, 46: 38835–38844.

26. Kartik Subramanian, Mark R Paul, and John J Tyson. 2015. Dynamical Localization of DivL and PleC in the Asymmetric Division Cycle of Caulobacter crescentus: A Theoretical Investigation of Alternative Models. *PLOS Computational Biology* 11, 7: e1004348.

27. Kartik Subramanian and John J Tyson. 2017. Spatiotemporal models of the asymmetric division cycle of Caulobacter crescentus. *Asymmetric Cell Division in Development, Differentiation and Cancer*: 23–48.

28. Benedetto Terrana and Austin Newton. 1975. Pattern of unequal cell division and development in Caulobacter crescentus. *Developmental biology* 44, 2: 380–385.

29. Carolina Tropini and Kerwyn Casey Huang. 2012. Interplay between the localization and kinetics of phosphorylation in flagellar pole development of the bacterium Caulobacter crescentus. *PLoS Comput Biol* 8, 8: e1002602.

30. Christos G Tsokos and Michael T Laub. 2012. Polarity and cell fate asymmetry in Caulobacter crescentus. *Current opinion in microbiology* 15, 6: 744–750.

31. Christos G Tsokos, Barrett S Perchuk, and Michael T Laub. 2011. A dynamic complex of signaling proteins uses polar localization to regulate cell-fate asymmetry in Caulobacter crescentus. *Developmental cell* 20, 3: 329–341.

32. Wei Zhao, Samuel W Duvall, Kimberly A Kowallis, Dylan T Tomares, Haley N Petitjean, and W Seth Childers. 2018. A circuit of protein-protein regulatory interactions enables polarity establishment in a bacterium. *bioRxiv*: 503250.